Heightened levels and seasonal inversion of riverine suspended sediment in a tropical biodiversity hot spot due to artisanal gold mining

Evan N. Dethier[a,1], Shannon L. Sartain[a], and David A. Lutz[b,c]

[a]Department of Earth Sciences, Dartmouth College, Hanover, NH 03755; [b]Environmental Studies Program, Dartmouth College, Hanover, NH 03755; and [c]Ecology, Evolution, Ecosystems, and Society Program, Dartmouth College, Hanover, NH 03755

Edited by Andrea Rinaldo, École Polytechnique Fédérale de Lausanne, Lausanne, Switzerland, and approved October 6, 2019 (received for review May 6, 2019)

In recent years, rising gold prices have exacerbated the global proliferation of artisanal-scale gold mining (ASGM), with catastrophic consequences for human and ecological health. Much of this burgeoning industry has occurred in biodiversity hot spots, notably in the tropical forests of South America. While the loss of tropical forests and floodplains as a result of ASGM has been well characterized, ASGM impacts on riverine hydrological properties are less understood. Previous fieldwork on ASGM-affected and gully-eroded tropical streams and rivers has demonstrated that increases in suspended-sediment concentration (SSC) can substantially impact fish diversity and aquatic community structure, yet our understanding of the timing and scope of impacts of such increases is limited by the lack of long-term records of SSC. To address this challenge, we present a 34-y analysis of the direct effect of ASGM on 32 river reaches in the Madre de Dios region of Peru, which has been heavily impacted by ASGM since the 1980s. We evaluate spatial and temporal patterns of impacts using estimated SSC derived from Landsat satellite imagery. We find that 16 of 18 stretches of river impacted by ASGM show significant increasing trends in SSC ($P < 0.05$), while only 5 of 14 unaffected sites do so. Additionally, ASGM appears to reverse natural seasonal cycles of SSC, which may imperil aquatic species. Overall, our findings indicate that ASGM is fundamentally altering optical water quality dynamics of a critical tropical biodiversity hot spot and provide guidance for future regulation of these activities.

tropical biodiversity hot spot | rivers | suspended sediment | remote sensing | Amazon

The rise of artisanal-scale gold mining (ASGM) is a global phenomenon with documented impacts on tropical forests and floodplains (e.g., refs. 1 and 2), including in the Madre de Dios River (MDDR) near the headwaters of the Madeira River, the largest tributary to the Amazon. Despite the potential sensitivity of aquatic systems to ASGM impacts (3, 4), the influence of mining activities on riverine processes in this region is not well known. Similar to other tropical moist forests that have been impacted by ASGM, the MDDR provides habitat for diverse ecological communities; sustains local human populations via commerce, via the provisioning of aquatic protein sources, and by providing a fresh water supply; and is an important conduit and repository for physical sediments (5) and dissolved organic carbon (6). Although tributaries to the MDDR are prone to dramatic daily variations throughout the year, discharge, sediment concentration, and organic matter transport on the main stem have relatively consistent seasonal variation (7), with low water and sediment concentrations during the dry season and elevated levels during the rainy season (8). As in many lowland areas, these seasonal patterns influence ecological and biogeochemical processes in channels and the riparian zone as well as ecological and human activity that occurs in the broader MDDR (9).

Episodic and seasonal flooding events in the MDDR influence the physiochemical properties of floodplains, and rapid meandering across floodplain zones leads to a patchwork landscape of terrestrial vegetation and permanently inundated lakes (10). The diversity of habitat structures on these floodplains and the surrounding terra firme forest ecosystems in the MDDR supports tremendous biodiversity (8, 11), including both unique endemic and threatened aquatic (12) and terrestrial (13) species. Furthermore, these floodplains are critical for the development of robust fisheries. Fish remains a crucial source of protein for local populations in the Peruvian Amazon (14), in some rural locations constituting nearly one-half of their animal-derived intake (15). However, these floodplains are generally the primary location for ASGM operations and therefore remain vulnerable to potential disturbance.

Intense ASGM activity has deforested greater than 100,000 ha of land in the MDDR (1) and has been detrimental to ecological and human health of proximal and downstream communities. The removal of forest biomass is a prerequisite for ASGM processes (16) and leads to increases in sediment concentration (17), turbidity (3), and conductivity (18) in nearby streams and rivers. After land appropriated for ASGM is cleared, physical separation of alluvial sediments in sluices and/or settling ponds is followed by mercury amalgamation and burning, allowing for the isolation of relatively pure gold. In the process, large quantities of mining

Significance

Artisanal-scale gold mining (ASGM) operations are expanding across the planet, leading to widespread riparian deforestation and excavation, and hastening sediment transport into nearby rivers. Here, we show that ASGM operations have led to major increases in river suspended-sediment concentrations across a wide region of the Peruvian Amazon. The magnitude of suspended-sediment increase we detect implies detrimental and long-lasting impacts on aquatic biota, particularly behavior and community structure of fish populations, and increased riverine transport of ASGM-contributed, mercury-laden sediments. Our data document that ASGM has rapidly decreased water quality in this large region since the 1980s, indicating a pressing need for biogeochemical and ecological evaluations of ASGM-affected rivers worldwide in order to quantify indirect consequences on aquatic species and human health.

Author contributions: E.N.D., S.L.S., and D.A.L. designed research; E.N.D. and S.L.S. performed research; E.N.D. contributed new reagents/analytic tools; E.N.D., S.L.S., and D.A.L. analyzed data; and E.N.D., S.L.S., and D.A.L. wrote the paper.

The authors declare no competing interest.

This article is a PNAS Direct Submission.

Data deposition: The data used in this analysis have been deposited at HydroShare, http://www.hydroshare.org/resource/0efe95f8326d497eb427e97a58b1b577/. Appropriate metadata are also included.

[1]To whom correspondence may be addressed. Email: evan.n.dethier.gr@dartmouth.edu.

This article contains supporting information online at www.pnas.org/lookup/suppl/doi:10.1073/pnas.1907842116/-/DCSupplemental.

First published November 11, 2019.

sediments and liquids, including mercury, are generally allowed to return to nearby streams and rivers. Mercury and other contaminants remain strongly associated with fine-grained sediment in affected waterways (19), bioaccumulating in fish tissues (20, 21) and entering human populations (22). There has been significant concern regarding potential health risks to local populations from ASGM-associated mercury-laden suspended sediments (14, 21, 23), yet the dynamics of mercury cycling in river systems is complex. Thus, in order to identify mercury-associated health risks to local populations, understand AGSM-related impacts on unique ecological communities in the Madre de Dios (MDD) region, and guide mitigation and regulation efforts for AGSM, it is critical to document the temporal dynamics of suspended sediments in ASGM-affected river systems such as the MDD.

In addition to the transport of mercury, increased aquatic suspended-sediment concentrations nearby ASGM operations have been seen to complicate the seasonal dynamics of physiochemical conditions of local streams and rivers. Many diverse neotropical fish communities are structured in ways that are associated with water clarity (24), with increases in turbidity and suspended sediment significantly influencing species assemblages in invertivores and surface fishes (3). ASGM-derived sediment often covers near-bank habitat (17) and can detrimentally impact aquatic macrophytes as well as primary producers such as diatoms (4). Furthermore, organisms dependent upon benthic macroinvertebrates, including ecologically and commercially important species such as catfishes in the Pimelodidae family and pacu and piranha species in the Serrasalmidae family (18), have been documented to be absent in the ASGM-impacted Inambari River in the MDDR. While there have been several attempts to document the degree to which the life history and behavior of aquatic species in the MDD watershed fluctuate in parallel with water volume and physiochemical conditions (7), these diverse communities are still in need of study. Consequently, temporal and seasonal documentation of changes to sediment regimes in the MDD due to ASGM is critical for assessing overall impacts to aquatic species and constructing effective conservation policies.

Altogether there are manifold needs for assessing the physiochemical impact of ASGM on tropical rivers over large spatial and long temporal scales. Satellite remote sensing has long been recognized as a technology that can reliably provide information regarding turbidity and suspended-sediment concentration (SSC) in aquatic environments (25, 26). Relationships between spectral reflectance and physical hydrological characteristics have been used to accurately document SSC in rivers, including in systems affected by ASGM (27). In this analysis, we expand the spatial and temporal scope of documenting SSC dynamics due to ASGM using satellite-derived estimates at 32 river reaches in the MDD watershed, taking 15,527 samples from 3,280 images in the 34-y Landsat record (Fig. 1). We present an accounting of the magnitude of ASGM impacts, including how those impacts alter the natural seasonality of affected tropical rivers in a biodiversity hot spot of global conservation concern. In doing so, we address the long-standing knowledge gap regarding SSC dynamics in aquatic ecosystems heavily impacted by ASGM. We provide a greater understanding of the degree to which aquatic communities and mercury dynamics may be influenced by continued ASGM operations in and along the MDDR.

Results

We observed increases in median annual SSC at all sites that we classified as "affected" by ASGM between 1984 and 2018. These increases were statistically significant ($P < 0.05$) at 16 of 18 (89%) affected sites (*SI Appendix*, Table S1). In contrast, sites that were classified as "unaffected" generally did not show statistically significant change in median annual SSC; only 5 of 14 sites (36%) showed significant change (*SI Appendix*, Table S1). In the most extreme case, annual SSC concentrations increased

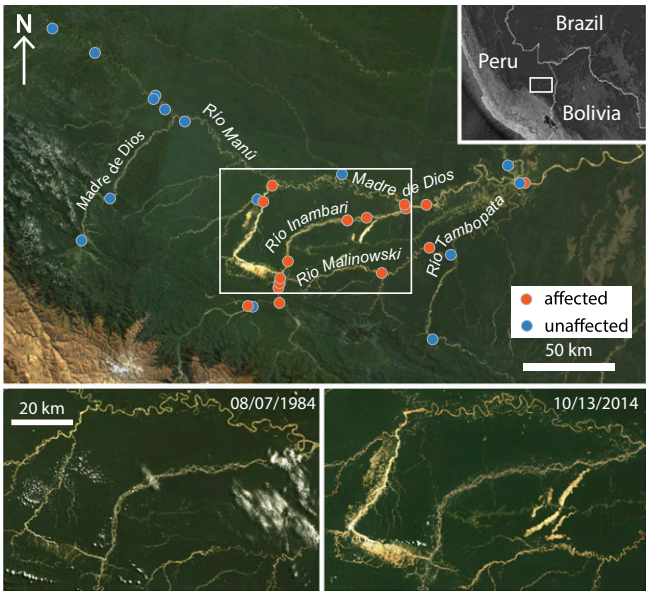

Fig. 1. Site map (*Upper*) shows a median composite Landsat 5 image from 2010 to 2013 with all 18 affected (orange markers) and 14 unaffected (blue markers) sites in the MDDR region analyzed for changes in SSC due to artisanal-scale gold mining. The *Lower* panel shows Landsat images pre- (*Left*) and post-ASGM (*Right*); rapid changes due to ASGM deforestation and mining operations are evident as large patches of highly reflective ground and water in the 2014 image (*Right*).

by nearly an order of magnitude (Fig. 2 *C* and *D*). Timing of SSC changes corresponds to changes in riparian deforestation due to ASGM activities, as mapped by Caballero Espejo et al. (1). Nonparametric Spearman correlation between median annual SSC and riparian deforestation shows significant positive relationships at 16 of 18 affected sites ($P < 0.05$). Increases in SSC were most pronounced at the onset of ASGM perturbation (Fig. 2, dashed lines); at some sites affected by ASGM, a straightforward relationship exists between median-annual SSC and percent riparian deforestation (e.g., *SI Appendix*, Fig. S2 *A* and *B*). However, at some sites, pronounced nonlinearities in SSC timeseries indicate more complexity in these relationships (e.g., *SI Appendix*, Fig. S2 *C* and *D*).

Notable in the trends of annual SSC at "affected" sites is that increases in SSC began directly following the onset of ASGM activity and have not abated through the present (Fig. 2). Only at Rio Colorado, the longest continuously affected site, have increases in median annual SSC waned in recent years; however, this recent trend follows a 2 order-of-magnitude increase in annual SSC in the decades prior (*SI Appendix*, Fig. S1). SSC thus remains elevated at this site compared to natural conditions. While unaffected sites do not indicate recent loading of sediment due to ASGM, fluctuations in SSC present over the time period of the study (e.g., Fig. 2*H*) may reflect changing hydrology and/or other anthropogenic disturbance to these tributaries.

Tributaries to the MDDR, like many other watersheds draining the Andes, exhibit significant natural interannual and intraannual variation in SSC, transporting higher SSCs during the wet months (January to April) and lower SSCs during the dry months (July to September). These dynamics are evident in our analysis in sites unaffected or not yet affected by ASGM (Fig. 2 and *SI Appendix*, Table S2). Across these sites, the median wet-season SSC is 2.76 times the median dry-season SSC; in contrast, following the onset of mining, SSC increases during the dry months, and affected sites have a median wet- to dry-season SSC ratio of only 1.28. Each of the 16 affected sites with statistically

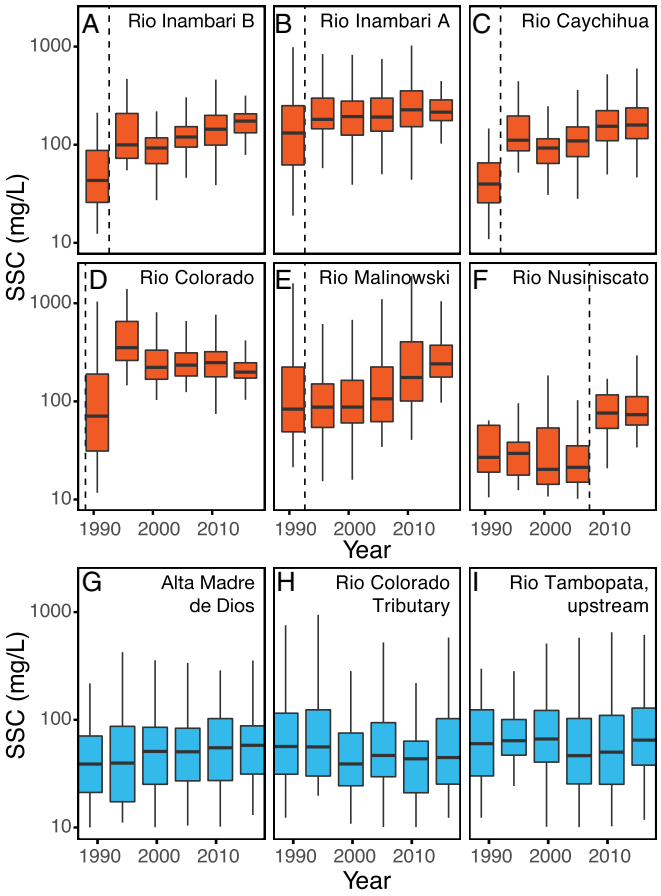

Fig. 2. Distribution of suspended-sediment concentration (SSC) (milligrams per liter; boxes indicate interquartile range, whiskers extend to the range of the data without outliers) for 6 sites in this study categorized as affected (*A–F*, orange) and 3 as unaffected (*G–I*, blue) by artisanal-scale gold mining (ASGM). The dashed lines indicate the first year with significant mining in the riparian zone. We report the significance of the Mann–Kendall trend test for these data. Of all affected sites, 16 of 18 show significant trends ($P < 0.05$), while only 5 of 14 unaffected sites show significant changes over this 34-y record.

significant annual trends is elevated in SSC during the dry months, with *t* tests indicating statistical significance ($P < 0.05$) at 13 sites relative to pre-ASGM. Although 12 of these 16 sites are elevated relative to pre-ASGM during the wet months, at only 5 sites are increases statistically significant ($P < 0.05$), indicating that ASGM influence on SSC is greatest during months in the dry season. Two sites (Rio Caychihua and Rio Colorado, upstream) with likely robust dry- and wet-season SSC increases are directly downstream of the Huepetuhe project and therefore have been influenced by ASGM for nearly the entire 34-y study period.

Aggregate analysis of SSC* (SSC normalized by the site-median SSC) at all affected sites shows a regional ASGM signature of elevated SSC* relative to pre-ASGM conditions, particularly in the dry season (Fig. 3). During the wet season, the median increase in SSC* is 1.05 to 1.20 times the pre-ASGM condition for the months of November and December ($P < 0.1$). During the dry season, SSC increase is greater; the median relative increase in SSC* is between 1.29 and 1.31 times pre-ASGM values and is statistically significant for each 2-mo grouping ($P < 0.05$).

Dry-season changes in SSC post-ASGM at individual sites corroborate the season-specific impacts of mining activity, particularly for those areas most significantly impacted by ASGM-related deforestation. For instance, an upper tributary to Rio Malinowski, which borders the Tambopata National Reserve that has been mined since 2016, showed a 256% dry-season increase from 53 to 190 mg/L. In some cases, such as along Rio Inambari, inversion of typical seasonal cyclicity in SSC has occurred, with higher SSC in the dry season than wet (Fig. 4). Similar impacts have likely occurred at Rio Colorado, the site most directly associated with activity at Huepetuhe and the Delta area (1). ASGM activity in the 1980s limits the number of pre-mining SSC estimates for those sites; the sparse available data indicate that increases in SSC may be 10-fold, from 44 to 800 mg/L in the dry season and 36 to 465 mg/L in the wet season. These estimates are supported by comparison to the major unaffected tributary to Rio Colorado, for which SSCs remain consistently an order-of-magnitude lower than the perturbed main stem following post-ASGM divergence in the early 1990s (*SI Appendix*, Fig. S1). Overall, while the degree of impact has varied considerably across individual sites, the onset of ASGM has led to significantly increased SSC with the highest concentrations often occurring in the dry season, which under natural conditions would be a time of low SSC.

Discussion

We attribute the observed increases in SSC at affected sites in the MDD solely to mining activity. Mining operations often sluice processed sediment directly to the channel or leave it in unconsolidated deposits that wash into the channel during precipitation and/or flooding events (28). In our analysis, few sites unaffected by ASGM show significant changes in SSC, even where land clearing for agriculture and/or infrastructure development has occurred (*SI Appendix*, Fig. S3 *A* and *B*). This is in

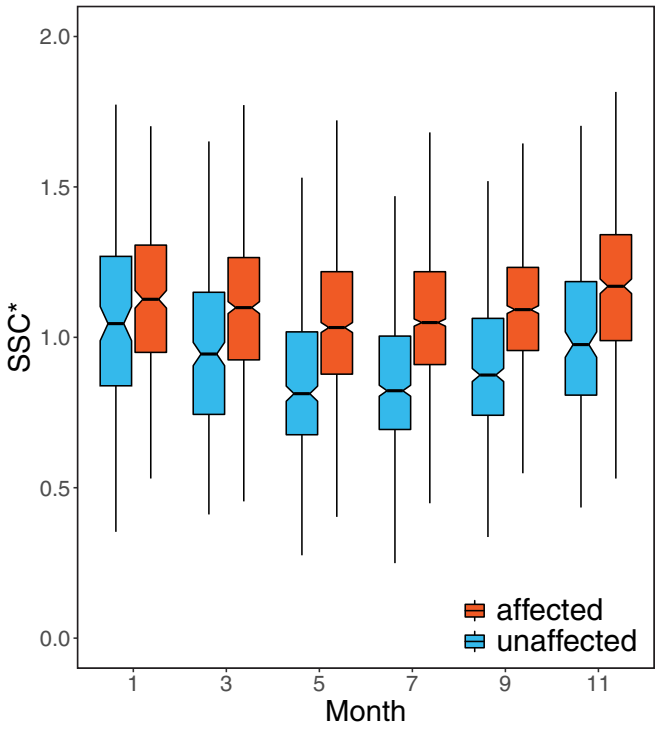

Fig. 3. Two-month aggregates of SSC* (SSC/site-median SSC) for all affected sites show increases post–artisanal-scale gold mining (ASGM) (orange) in each season relative to pre-ASGM conditions (blue). These increases are statistically significant (*t* test, $P < 0.05$) during each period, but greater unaffected–affected disparity is observed during the dry-season period. The boxes indicate interquartile range; the whiskers extend to the range of the data without outliers.

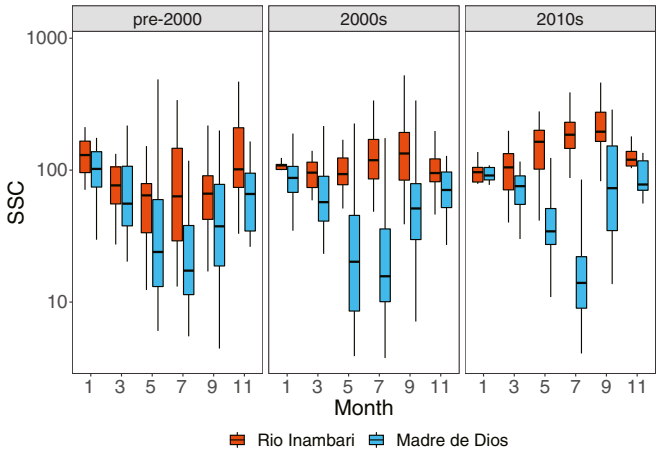

Fig. 4. Natural seasonal variability on the unaffected Upper MDDR (blue boxes) illustrates the pattern of higher suspended-sediment concentration (SSC) during the wet season and low SSC during the dry season. This seasonality is also evident pre-ASGM operations on Rio Inambari (orange boxes), where significant mining began in the early 1990s. Post-ASGM (2000s), the typical SSC is higher than pre-ASGM, although this increase is only statistically significant (pooled *t* test, $P < 0.05$) in the dry months. In the 2010s, high dry-season SSC due to expansion of upstream mining activity has inverted the typical annual SSC cycle. The boxplots show SSC interquartile range calculated for each 2-mo period for all observations in the specified decade. The whiskers indicate the range of the data excluding outliers.

contrast to studies showing elevated sediment yields as a result of deforestation and agriculture in other tropical locales (29). In the MDDR, nonmining disturbance may not occur directly in the river channel or floodplain, and its signature may thus be dampened relative to that of ASGM (*SI Appendix*, Fig. S3 *C–E*). We do observe significant trends at 5 pristine/unaffected sites, possibly the result of increasing runoff from the Andean highlands over time or upstream deforestation. Coupled terrestrial and hydrological modeling is needed to fully discern these drivers.

Sediment contamination is a well-documented impact of mining activities (3, 28, 30). Many contaminants, including mercury, preferentially sorb to fine-grained particles (19, 30). In this case, mercury contamination likely stems both from in situ sources and addition during the amalgamation process. The subsequent association with fine sediment allows for riverine transmission, as well as increased bioavailability (31), leading to direct incorporation into cell tissue of fish and thus rapid and irreversible bioaccumulation (22). We demonstrate the pervasiveness of elevated SSCs due to mining impacts in the region, which helps to explain the widespread mercury contamination found in fish (20, 21) and human (22) populations in the MDDR.

In some instances of mining pollution, contamination stems from a single point and/or event source (30). Impacts in these cases may be locally catastrophic only in the short term. In cases where contaminant inputs are limited in space and/or time, in-channel recovery by natural river processes can be relatively rapid and occur on annual to decadal timescales. However, widespread and prolonged mining such as that in the MDDR likely leads to "hot spots" at source areas, as well as in-channel and floodplain deposits. These hot spots may remain elevated for more than a century after cessation of mining (32). There is no indication that mining activity will slow in the near term, and rivers in the MDDR migrate frequently. It thus seems likely that regular reworking of contaminated sediments will last for decades even after the eventual cessation of mining activities (33), thereby complicating efforts to prevent mercury from entering nearby ecological communities and food systems.

One question surrounding mercury-bound sediments in the MDDR relates to the spatial pervasiveness of contaminated particles downstream from ASGM sites. Limited increase in SSC found in sites >50 km downstream of ASGM activity (e.g., MDD, downstream 2) indicates that SSC impacts are most pronounced immediately downstream of mining operations (e.g., Rio Colorado, Rio Malinowski). Proximal to mining, increases in SSC have changed many tributary streams from intermittently clear to consistently muddy. Significantly increasing trends in SSC have not appeared to level off except at the most affected sites (Rio Colorado upstream and Rio Caychihua, both immediately downstream of the Huepetuhe project), and only after an order-of-magnitude increase in dry-season SSC. The impact of ASGM on waters much farther downstream is more nuanced. Marked increase in SSC began in 1996 at the downstream-most Rio Inambari site, coincident with major operations at Huepetuhe ∼100 km upstream (1) and more than a decade before more proximal operations affected that system. A slight, but statistically significant, increase in SSC along the main stem of the MDDR has occurred over the period of observation. Nonimpacted tributaries to the MDD likely dilute contaminant and physical pollution on the main stem; however, the area of impacted land upstream continues to increase (1), limiting this dilution, delaying recovery, and increasing the total flux of contaminated sediments transported downstream. Numerous dams planned for the headwaters of the Amazon River, including in the Madeira region, threaten to severely reduce downstream sediment discharge, perhaps further limiting the diluting effects of uncontaminated sediment delivered from the mountains.

Reanalysis of data collected in ASGM-affected watersheds in Brazil (34) and in the MDD (20) indicates mercury concentrations in ASGM-associated suspended sediment are elevated roughly 5 times above suspended sediment from unaffected sites (*SI Appendix*, Fig. S4). Contamination is likely amplified by elevated SSC concentrations; as a result, mercury concentrations may be elevated downstream of affected sites by an order of magnitude or more. A conservative analysis using predicted average mercury concentration and average annual discharge suggests that a metric ton of mercury may be input to the main stem of the MDD from ASGM-affected tributaries each year, relative to a negligible pre-ASGM flux. Targeted field study is required to determine the speciation and fate of this mercury; however, the combination of excess supply to rivers and potential for anoxia due to increased sediment loading may increase the likelihood of methylation. Sediments, fish, and human populations sampled downstream show elevated levels of mercury relative to upstream of ASGM influence (20). These findings suggest that, following initial pulses of ASGM expansion, mercury-related impacts may be prolonged due to exposed sediments being easily mobilized. Further research into the spatial and temporal dynamics of sediments from unique mining sites at fine scales is warranted to better understand these processes.

In addition to contaminant pollution resulting from heavy metal use, ASGM sites produce physical sediment pollution that can change the grain size and geometry of the channel bed and critically limit light penetration (35, 36). In the MDD, ASGM activity has led to the systematic alteration of sediment transport. Van Nieuwenhuyse and LaPerriere (35) found that high turbidity in affected streams can substantially diminish (moderate mining, turbidity: 110 to 230 nephelometric turbidity units [NTU]) or extinguish (heavy mining, turbidity: >500 NTU) primary productivity (35). We used an empirical relationship between SSC and turbidity to estimate that turbidity levels at affected sites in the MDD are between 150 and 2,000 NTU, even in the dry season (*SI Appendix*, Fig. S5). Excess turbidity can also affect vertebrate populations by limiting visibility and/or affecting respiration, thus altering species hierarchies, and limiting territory defense and feeding success (3, 37). While rates of fish kill from

elevated turbidities vary based on species, it is likely that fish living in streams with clear water prior to ASGM initiation are poorly adapted to year-round high SSC conditions post-ASGM (36). Research into MDDR fish populations post-ASGM indicate that SSC conditions can radically transform species abundances (18, 28). Further collections, made in conjunction with our findings, may help elucidate species-specific responses and help understand special areas of conservation concern.

Prolonged above-average SSC may lead to deposition of excess sediments on riverbeds, riverbanks, and floodplains, altering grain size and increasing embeddedness (3). These thick layers of fine sediment on channel bottoms can limit hyporheic exchange and impact macroinvertebrate populations as well as reduce/homogenize stream habitat (3). For most sites in the MDDR, changes have occurred primarily during the dry season, when mining operations are most active and natural SSCs are low. These changes will likely compound the impacts of increased SSC and contamination by stressing biota at varying trophic levels with life cycles attuned to seasonal cycles in SSC (38). For instance, migratory catfish species spawn during high-flow periods and young individuals inhabit lowland floodplains that serve as nurseries (7, 39). According to our results, these zones are likely detrimentally impacted during this critical rearing period, suggesting the potential for both top-down and bottom-up trophic cascades. Given that environmental cues are closely linked to neotropical fish behavior and life history strategies, there is a clear need for further research into the effects of ASGM SSC impacts on these aquatic species. Visually oriented vulnerable and endangered species, such as the giant otter, *Pteronura brasilensis*, may also be considerably impacted by ASGM hydrological disturbance (40).

The direct input of mercury-contaminated sediments to rivers in the MDDR due to ASGM threatens ecological and public health; other investigators have found that contaminant impacts extend downstream potentially greater than 100 km (20). Although our research suggests that changes in SSC are so far most pronounced immediately downstream of ASGM operations, the unchecked expansion of these projects appears likely to continue to extend the severity of these impacts for the foreseeable future. We provide a valuable first step in understanding the previously underexplored hydrological footprint of ASGM in the MDDR, as well as a framework for further evaluating impacts at these and other affected regions. Our findings suggest that immediate and multidisciplinary research is needed to understand the full ecological and biogeochemical consequences of the increased sediment transport in this area.

Methods

Developing a Suspended-Sediment Detection Algorithm. To develop a calibration relating optical properties of river bodies to their SSC, we established individual algorithms for sites with adequate paired in situ measurements and satellite images from NASA's Landsat 5 and 7 missions. At several stations in the Amazon River Basin, the Brazilian Agência Nacional de Águas (ANA) (41) has collected suspended-sediment samples using surface sampling approximately twice monthly since 2000. They have conducted supplemental depth-integrated sampling projects to relate surface SSC to depth-integrated SSC, and we use the resulting depth-integrated values for our empirical remote-sensing methods. We used the Google Earth Engine platform to select Landsat US Geological Survey (USGS) L1T surface reflectance images acquired ±9 d from those in situ measurements at 13 ANA stations (*SI Appendix*, Table S6). For each image, we masked out pixels with image artifacts, and those classified by NASA as clouds, shadow, or snow/ice. We used a normalized difference water index with the near-infrared and blue wavelengths to select only channel water pixels from the remaining pixels of each image. Finally, for each image of each station, we sampled the channel water pixels within a 500-m radius of the station coordinates, calculating a median value for each Landsat wavelength band.

The varying mineralogy of river sediment in different systems reduces the accuracy of algorithms trained with data from other systems (42). Thus, we used *K*-means clustering to automate the classification of each river as one of 3 categories, based on its decadal average surface reflectance in bands 1 and 3, and 2 ratios: B4/B1 and B3/B1, parameters selected using principal-component analysis. The clustering analysis automatically groups rivers with similar typical spectral reflectance characteristics, which are the result of carrying similar sediment types and/or concentrations. Dividing rivers into types allows for calibration development and implementation specific to each river type, thus reducing bias due to interriver variation. For each *K*-means group, we constructed linear models using cross-validated lasso regression to select variables from a list of spectral reflectance bands and band ratios (*SI Appendix*, Table S1), developing empirical relationships between band optical properties and the log-transformed SSC. We tested regression model success on holdout sets comprising 25% of the data (average relative error, 24%; total $n = 2{,}028$) (*SI Appendix*, Fig. S6*A* and Table S3). The algorithms perform well in general, and specifically for the rivers in the MDD region (e.g., *SI Appendix*, Fig. S6*B*).

Estimating Trends in SSC and Mining Activity. To establish whether each river stretch was affected by ASGM or part of our unaffected control group, we used an annual dataset of ASGM mining extent in the MDD from 1984 to 2019 (1). For each site and year, we determined whether ASGM operations were ongoing in a 2-km riparian buffer around the channel centerline for all main stem and tributary streams <80 km upstream of the sampling site. We used Landsat, DigitalGlobe, and Planet Labs imagery for visual analysis of the resulting timeseries of upstream ASGM activity and to confirm the distinction between mining and other anthropogenic and natural disturbance. We classified river sites as "affected" or "unaffected" by ASGM based on whether the percent upstream deforestation in the riparian zone exceeded 0.05% (*SI Appendix*, Fig. S3 and Table S4), recording the first year that threshold was crossed.

For each image of the MDD region in the Landsat record (1984 to present), we applied the clustering function and the SSC algorithm to calculate SSC for the entire length and width of each river wider than 90 m. Data used for calibration and analysis are collected on Hydroshare (http://www.hydroshare.org/resource/0efe95f8326d497eb427e97a58b1b577/) (43). We selected 32 sites for analysis, including 18 downstream of mining activity and 14 control sites upstream of mining activity or in the long-preserved Manu National Park. At each site, we delineated a short (~2-km) transect along the river path. We sampled the water pixels in a 100-m buffer zone around that path to calculate SSC for each day with cloud-free imagery. Challenges posed by sparse data at some locations, particularly early in the Landsat record (*SI Appendix*, Fig. S7), were addressed by eliminating preliminary sites with sparse data (<150 noncloudy images) and aggregating data at our final sites on monthly, annual, and decadal time frames relevant to each analysis. These efforts generated sufficient imagery for each aggregation period to incorporate inherent variability in SSC and facilitate robust statistical analysis. To avoid sampling bias, we ensured that the ratio of wet- to dry-month images remained relatively uniform throughout the record, even when the total number of images varied. We confirmed the validity of our timeseries approaches by analyzing data generated by the same approach at affected and unaffected (control) sites.

For each study site, we calculated the annual median SSC from 1984 to 2018. In most cases, trends were monotonic but normality was not assured, so we conducted nonparametric Mann–Kendall trend test for each site time series. Because of the importance of seasonal variations in the water cycle, we also calculated the decadal geometric mean of SSC for each of 6 2-mo pairs (e.g., grouping January and February observations). We used decadal 2-mo groupings for selecting sufficient images for each analysis, while preserving interannual and intraannual information vital to understanding changes occurring in the MDD in the past 3 decades.

Because of the nonlinearity of some changes we observed in MDDR sites, we divided the record of each site into premining and postmining epochs based on our recorded year of mining onset (*SI Appendix*, Table S1). At each site, we calculated pre- and post-ASGM geometric mean SSC for each 2-mo period to further evaluate the seasonal component of ASGM influence. To compare sites with different background sediment transport dynamics, we normalized each SSC measurement by the median SSC at that site. We refer to this parameter as SSC*, and analyzed temporal trends in SSC* to determine the characteristic changes in SSC across the MDD region.

Contextualizing Suspended Sediment and Mercury Concentrations. To contextualize the changes observed in SSC, we conducted an analysis of turbidity using a USGS dataset of 18,568 paired turbidity and SSC measurements. We developed a relationship between SSC and turbidity (*SI Appendix*, Fig. S5), which constrained the likely turbidity in sites affected by ASGM, given estimates of SSC from our remote-sensing approach. As is evident in *SI Appendix*, Fig. S5, the range of SSC and inferred turbidity measurements is

within the typical range of rivers within the United States. Measurements made downstream of the MDDR on the Madeira River indicate a similar SSC range of ∼0 to 1,000 mg/L. Turbidity and SSC at these sites are thus not atypical of some natural systems; however, the observed changes in those parameters following the initiation of mining in the MDDR are atypical and suggest a fundamental alteration in affected rivers. These changes are the focus of this study.

We sought to estimate the increase in mercury resulting from elevated suspended sediment. Although direct measurements of mercury-associated with suspended sediment are sparse for the region, Telmer et al. (34) measured mercury and SSC downstream of ASGM activity in Brazil, and Diringer et al. (20) measured within our study area, both upstream and downstream of ASGM in the MDDR. We reanalyzed these data using multiple regression to generate regional relationships between log-transformed SSC and mercury concentration (Hg, nanograms per liter) at affected and unaffected locations (*SI Appendix*, Fig. S4). Although scattered ($r^2 = 0.62$), these relationships indicate a proportional relationship between SSC and mercury concentration; mercury concentration is significantly higher for a given SSC at ASGM-affected sites relative to unaffected sites (*SI Appendix*, Table S4). The datasets do not uniformly quantify distance from ASGM source, but high outlier values in the "affected" group are likely more proximal to ASGM, while low outliers are likely minimally affected by ASGM (34).

Following Telmer et al. (34), we generated conservative estimates of pre- and post-ASGM mercury flux at each affected river location in our dataset by multiplying the median annual at-a-station SSC by average annual discharge (44). To ensure uniformity, at-a-station discharge was estimated by scaling downstream average annual discharge (measured on the Madeira River at Porto Velho Station) by relative drainage area. Because annual discharge is held constant for a given site, in this simple analysis interannual variation in estimated mercury flux depends entirely on variations in SSC. By using the pre- and post-ASGM relationships between SSC and mercury concentration, we provide a means for estimating mercury fluxes before and after mining activity began.

Data Availability. The data used in this project are publicly available. We used data from the NASA Landsat missions (https://www.usgs.gov/land-resources/nli/landsat), accessed through the Google Earth Engine platform (https://earthengine.google.com/), as described in the text or at http://www.hydroshare.org/resource/0efe95f8326d497eb427e97a58b1b577/ (43). In situ data sources are cited in the text.

ACKNOWLEDGMENTS. The Dartmouth College Earth Science Department and the National Science Foundation (Grants EAR-1545623 and BCS-1636415) supported this project. We are grateful for the helpful guidance of Francis Magilligan, Carl Renshaw, and Miles Silman throughout and for Jorge Caballero Espejo for providing shapefiles of deforestation in the MDD area.

1. J. Caballero Espejo *et al*., Deforestation and forest degradation due to gold mining in the Peruvian Amazon: A 34-year perspective. *Remote Sens.* **10**, 1903 (2018).
2. G. P. Asner, W. Llactayo, R. Tupayachi, E. R. Luna, Elevated rates of gold mining in the Amazon revealed through high-resolution monitoring. *Proc. Natl. Acad. Sci. U.S.A.* **110**, 18454–18459 (2013).
3. J. H. Mol, P. E. Ouboter, Downstream effects of erosion from small-scale gold mining on the instream habitat and fish community of a small neotropical rainforest stream. *Conserv. Biol.* **18**, 201–214 (2004).
4. L. Tudesque, G. Grenouillet, M. Gevrey, K. Khazraie, S. Brosse, Influence of small-scale gold mining on French Guiana streams: Are diatom assemblages valid disturbance sensors? *Ecol. Indic.* **14**, 100–106 (2012).
5. R. Kalliola, M. Puhakka, J. Salo, A. Linna, M. Räsänen, Mineral nutrients in fluvial sediments from the Peruvian Amazon. *Catena* **20**, 333–349 (1993).
6. X. Feng *et al*., Source to sink: Evolution of lignin composition in the Madre de Dios River system with connection to the Amazon basin and offshore. *J. Geophys. Res. Biogeosci.* **121**, 1316–1338 (2016).
7. C. M. Cañas, W. E. Pine, Documentation of the temporal and spatial patterns of Pimelodidae catfish spawning and larvae dispersion in the Madre de Dios River (Peru): Insights for conservation in the Andean-Amazon headwaters. *River Res. Appl.* **27**, 602–611 (2011).
8. M. Thieme *et al*., Freshwater conservation planning in data-poor areas: An example from a remote Amazonian basin (Madre de Dios River, Peru and Bolivia). *Biol. Conserv.* **135**, 500–517 (2007).
9. S. K. Hamilton, J. Kellndorfer, B. Lehner, M. Tobler, Remote sensing of floodplain geomorphology as a surrogate for biodiversity in a tropical river system (Madre de Dios, Peru). *Geomorphology* **89**, 23–38 (2007).
10. J. A. Constantine, T. Dunne, J. Ahmed, C. Legleiter, E. D. Lazarus, Sediment supply as a driver of river meandering and floodplain evolution in the Amazon Basin. *Nat. Geosci.* **7**, 899–903 (2014).
11. F. H. Valverde, J. Janovec, M. Tobler, Floristic diversity and composition of terra firme and seasonally inundated palm swamp forests in the Palma Real watershed in lower Madre de Dios, Peru. *SIDA Contrib. Bot.* **22**, 615–633 (2006).
12. R. S. A. Pickles *et al*., Genetic diversity and population structure in the endangered giant otter, *Pteronura brasiliensis*. *Conserv. Genet.* **13**, 235–245 (2012).
13. T. M. Doan, W. Arizabal Arriaga, Microgeographic variation in species composition of the herpetofaunal communities of Tambopata region, Peru. *Biotropica* **34**, 101–117 (2002).
14. K. A. Roach, N. F. Jacobsen, C. V. Fiorello, A. Stronza, K. O. Winemiller, Gold mining and mercury bioaccumulation in a floodplain lake and main channel of the Tambopata River, Peru. *J. Environ. Prot.* **4**, 51–60 (2013).
15. M. E. McClain, R. E. Cossío, The use of riparian environments in the rural Peruvian Amazon. *Environ. Conserv.* **30**, 242–248 (2003).
16. K. M. Wantzen, Physical pollution: Effects of gully erosion on benthic invertebrates in a tropical clear-water stream. *Aquat. Conserv.* **16**, 733–749 (2006).
17. K. Wantzen, J. Mol, K. M. Wantzen, J. H. Mol, Soil erosion from agriculture and mining: A threat to tropical stream ecosystems. *Agriculture* **3**, 660–683 (2013).
18. N. K. Lujan *et al*., Aquatic community structure across an Andes-to-Amazon fluvial gradient. *J. Biogeogr.* **40**, 1715–1728 (2013).
19. E. V. Axtmann, S. N. Luoma, Large-scale distribution of metal contamination in the fine-grained sediments of the Clark Fork River, Montana, U.S.A. *Appl. Geochem.* **6**, 75–88 (1991).
20. S. E. Diringer *et al*., River transport of mercury from artisanal and small-scale gold mining and risks for dietary mercury exposure in Madre de Dios, Peru. *Environ. Sci. Process Impacts* **17**, 478–487 (2015).
21. G. Martinez *et al*., Mercury contamination in riverine sediments and fish associated with artisanal and small-scale gold mining in Madre de Dios, Peru. *Int. J. Environ. Res. Public Health* **15**, E1584 (2018).
22. A. L. Langeland, R. D. Hardin, R. L. Neitzel, Mercury levels in human hair and farmed fish near artisanal and small-scale gold mining communities in the Madre de Dios River Basin, Peru. *Int. J. Environ. Res. Public Health* **14**, E302 (2017).
23. K. E. Markham, F. Sangermano, Evaluating wildlife vulnerability to mercury pollution from artisanal and small-scale gold mining in Madre de Dios, Peru. *Trop. Conserv. Sci.* **11**, 194008291879432 (2018).
24. S. Mérigoux, B. Hugueny, D. Ponton, B. Statzner, P. Vauchel, Predicting diversity of juvenile neotropical fish communities: Patch dynamics versus habitat state in floodplain creeks. *Oecologia* **118**, 503–516 (1999).
25. R. Espinoza Villar *et al*., The integration of field measurements and satellite observations to determine river solid loads in poorly monitored basins. *J. Hydrol.* **444–445**, 221–228 (2012).
26. T. M. Pavelsky, L. C. Smith, Remote sensing of suspended sediment concentration, flow velocity, and lake recharge in the Peace-Athabasca Delta, Canada. *Water Resour. Res.* **45**, W11417 (2009).
27. F. Lobo, M. Costa, E. Novo, K. Telmer, Distribution of artisanal and small-scale gold mining in the Tapajós River Basin (Brazilian Amazon) over the past 40 Years and relationship with water siltation. *Remote Sens.* **8**, 579 (2016).
28. G. Balamurugan, Tin mining and sediment supply in peninsular malaysia with special reference to the Kelang River Basin. *Environmentalist* **11**, 281–291 (1991).
29. T. Hewawasam, F. von Blanckenburg, M. Schaller, P. Kubik, Increase of human over natural erosion rates in tropical highlands constrained by cosmogenic nuclides. *Geology* **31**, 597 (2003).
30. W. Salomons, A. M. Eagle, Hydrology, sedimentology and the fate and distribution of copper in mine-related discharges in the fly river system, Papua New Guinea. *Sci. Total Environ.* **97–98**, 315–334 (1990).
31. M. Stone, J. Marsalek, Trace metal composition and speciation in street sediment: Sault Ste. Marie, Canada. *Water Air Soil Pollut.* **87**, 149–169 (1996).
32. M. B. Singer *et al*., Enduring legacy of a toxic fan via episodic redistribution of California gold mining debris. *Proc. Natl. Acad. Sci. U.S.A.* **110**, 18436–18441 (2013).
33. T. J. Coulthard, M. G. Macklin, Modeling long-term contamination in river systems from historical metal mining. *Geology* **31**, 451 (2003).
34. K. Telmer, M. Costa, R. Simões Angélica, E. S. Araujo, Y. Maurice, The source and fate of sediment and mercury in the Tapajós River, Pará, Brazilian Amazon: Ground- and space-based evidence. *J. Environ. Manage.* **81**, 101–113 (2006).
35. E. E. Van Nieuwenhuyse, J. D. LaPerriere, Effects of placer gold mining on primary production in subarctic streams of Alaska. *J. Am. Water Resour. Assoc.* **22**, 91–99 (1986).
36. M. E. Kjelland, C. M. Woodley, T. M. Swannack, D. L. Smith, A review of the potential effects of suspended sediment on fishes: Potential dredging-related physiological, behavioral, and transgenerational implications. *Environ. Syst. Decis.* **35**, 334–350 (2015).
37. L. Berg, T. G. Northcote, Changes in territorial, gill-flaring, and feeding behavior in juvenile coho salmon (*Oncorhynchus kisutch*) following short-term pulses of suspended sediment. *Can. J. Fish. Aquat. Sci.* **42**, 1410–1417 (2008).
38. G. S. Bilotta, R. E. Brazier, Understanding the influence of suspended solids on water quality and aquatic biota. *Water Res.* **42**, 2849–2861 (2008).
39. C. A. R. M. Araujo-Lima, E. C. Oliveira, Transport of larval fish in the Amazon. *J. Fish Biol.* **53**, 297–306 (2005).
40. F. C. W. Rosas, J. A. S. Zuanon, S. K. Carter, Feeding ecology of the giant otter, *Pteronura brasiliensis*. *Biotropica* **31**, 502–506 (1999).
41. Agência Nacional de Águas (ANA), HidroWeb: Sistema de Informações Hidrológicas (2017). http://www.snirh.gov.br/hidroweb/publico/apresentacao.jsf. Accessed 6 May 2019.
42. J.-M. Martinez, R. Espinoza-Villar, E. Armijos, L. Silva Moreira, The optical properties of river and floodplain waters in the Amazon River Basin: Implications for satellite-based measurements of suspended particulate matter. *J. Geophys. Res. Earth Surf.* **120**, 1274–1287 (2015).
43. E. Dethier, Madre de Dios Landsat-derived SSC estimates. HydroShare. http://www.hydroshare.org/resource/0efe95f8326d497eb427e97a58b1b577. Deposited 4 October 2019.
44. B. M. Fekete, C. J. Vörösmarty, W. Grabs, High resolution fields of global runoff combining observed river discharge and simulated water balances. *Global Biogeochem. Cycles* **16**, 15-11–15-10 (2002).